COBEM 2023 27TH INTERNATIONAL CONGRESS OF MECHANICAL ENGENEERING

ABCM Brazilian Society of Mechanical Sciences and Engineering
27th ABCM International Congress of Mechanical Engineering
December 04-08, 2023, Florianópolis-SC, Brazil

COB-2023-1550 - ANALYSIS OF AEROELASTIC STABILITY OF VISCOELASTIC SANDWICH PANELS IN SUBSONIC REGIME USING THE NONPLANAR DOUBLET-LATTICE METHOD

Bruno Sousa Carneiro da Cunha
Federal University of Uberlândia
brunocarneirocunha@ufu.br

Antônio Marcos Gonçalves de Lima
Federal University of Uberlândia
amglima@ufu.br

Abstract. *The engineers of aeronautical industries are frequently facing with subsonic panel flutter phenomena, where the design and analyses of aerospace vehicles requires the knowledge of their critical flutter speeds for safety requirements and to avoid catastrophes. Thus, whenever possible it is important to evaluate efficient and low-cost aeroelastic control strategies to deal with the problem of panel flutter phenomenon. In this context, the use of passive constraining viscoelastic layers seems to be an interesting alternative to be used in such situations. However, the structural and aerodynamic modeling procedures of an aeroviscoelastic system subjected to a subsonic airflow are not easy. In most of the cases, the difficult is related to the fact that, the viscoelastic behavior depends strongly on the excitation frequency and temperature, resulting in some difficulties during the coupling between the structural and aerodynamic models to account for the unsteady aerodynamics and complex behavior of the viscoelastic part, simultaneously. In this study, it is proposed an efficient numerical strategy to model aeroviscoelastic systems under subsonic airflows for panel flutter suppression. Here, the curved plate model of a thin three-layer sandwich panel and aerodynamic loadings using the nonplanar doublet lattice method are constructed both in MATLAB® environment code. Also, to solve the resulting equations of motion of the complex aeroviscoelastic system, a modified version of the pk method is proposed herein to estimate the critical flutter speeds and to verify the possibility of increasing the critical flutter speeds of the base panel by using viscoelastic materials. The influence of design parameters characterizing the performance of the viscoelastic treatment and its operation temperature on the flutter boundary has also been addressed herein.*

Keywords: *Nonplanar Doublet-lattice method, flutter suppression, viscoelastic materials, unsteady aerodynamic, aeroviscoelastic system*

1. INTRODUCTION

Numerous researchers in the public domain (Botez et al.,2003),(Brendel and Sulaeman, 1994),(Cunha et al., 2017),(Ingram and Szwarc, 1976), (Moon and Kim, 2001) have investigated the problem of panel flutter suppression with the aim of enhancing the stability of aeroelastic systems and preventing disasters. In this context, given the widespread use of viscoelastic layers (CVLs) for effectively mitigating undesired vibrations and noise in various industrial applications (Bagley and Torvik, 1983) and (Galucio and Deü, 2004), it is anticipated that this passive control technique can also be advantageously applied to suppress flutter phenomena, as demonstrated in (Cunha-Filho et al.,2016) for supersonic airflows. However, there have been limited efforts devoted to proposing a modeling methodology and conducting an analysis of aeroelastic problems that involve passive CVLs subjected to subsonic airflows, which serves as the motivation for this study. To accomplish this objective, the finite element method (FEM) will be employed in conjunction with the nonplanar Doublet-Lattice method (nDLM) to model the aeroviscoelastic system under investigation.

Currently, it is crucial to highlight that the Doublet-Lattice method offers distinct advantages over various aerodynamics modeling techniques documented in the literature. One key advantage is its capability to handle multiple lift surfaces, coupled with its low computational cost in comparison to high-fidelity computational fluid dynamics (CFD) models. This explains why it remains widely employed in aeronautical and aerospace industries for conducting aeroelastic analyses, particularly during the preliminary design stages, even when dealing with intricate aircraft configurations.

In the pursuit of utilizing viscoelastic materials for the purpose of mitigating flutter, most of the studies available in the literature primarily focus on the application of such materials under supersonic panel flutter conditions. These studies typically employ methodologies like the linear Piston theory to model aerodynamic loads (Cunha-Filho et al.,2016). As an example, (Merret and Hilton,2010) conducted an analytical investigation into the impact of viscoelastic damping treatment on the supersonic flutter speed of a plate, examining both the time and frequency domains. Additionally,

(Cunha-Filho et al.,2016) demonstrated the feasibility of employing passive CVLs to enhance the critical flutter speeds of a flat panel exposed to supersonic airflow. Importantly, their approach takes into account the frequency- and temperature-dependent characteristics of the viscoelastic component.

When considering practical applications, the utilization of surface viscoelastic treatments offers distinct advantages over other passive control methods. These advantages include inherent stability, effectiveness across a broad frequency range and low costs associated with their application and maintenance (Lima et al.,2009,2010). However, it is essential to acknowledge the sensitivity of these materials to operational and environmental variations. To ensure their maximum efficiency and establish limitations for a desired aeroelastic application, this sensitivity must be appropriately addressed during the modeling process. Nevertheless, it is worth noting that most modeling efforts concerning aeroelastic systems incorporating viscoelastic materials for flutter suppression have primarily relied on linearized and/or simplified methods, such as the widely used linear Piston theory employed in applications involving supersonic airflows (Lighthill,1953). Another commonly employed technique for addressing this type of aeroviscoelastic problem is the Strip theory (Bismarck-Nasr,1991), which provides the necessary increment in aerodynamic loading to predict the flutter boundary of an aeroviscoelastic system.

Nonetheless, accurately estimating the critical flutter speeds of an aeroviscoelastic system under subsonic airflows remains a challenging task when employing an unsteady aerodynamic modeling methodology like the nDLM (Blair, 1994). This challenge arises from the inherent complexity associated with the frequency- and temperature-dependent behavior of the viscoelastic component when coupling the viscoelastic structure with the unsteady aerodynamics acting upon it. Furthermore, appropriate modifications to the classical pk method (Hassig,1971) must be applied to adequately account for the frequency- and temperature-dependent complex stiffness matrix of the aeroviscoelastic problem. These modifications are necessary to achieve precise estimation of the system's flutter boundary.

Therefore, this paper presents a novel numerical modeling methodology to address the challenges associated with aeroviscoelastic systems under subsonic airflows for flutter suppression. In this methodology, the Finite Element Method (FEM) is employed to model a curved sandwich panel structure, while the nonplanar Doublet-Lattice Method (nDLM) is utilized to generate unsteady aerodynamic loadings. Another point of this study is the incorporation of Roger's approximation to construct the generalized aerodynamic matrix (GAM) and a modified version of the pk method. This approach effectively solves the resulting complex eigenvalue problem of the aeroviscoelastic system and accurately predicts the flutter boundary.

2. BACKGROUND ON THE NDLM METHOD

In the nonplanar DLM method, the dimensionless normalwash is expressed as follows Rodden et al. (1998):

$$w(x,s)=\frac{1}{8\pi}\sum_{n=1}^{N}\iint_{S_n}K(x,\xi,s,\sigma)\,p(\xi,\sigma)\,d\xi\,d\sigma \tag{1}$$

where $p(\xi,\sigma)$ is the complex amplitude of the lifting pressure coefficient, (x,s) are the orthogonal coordinates on the *n*th surface, S_n , and K is the kernel function for oscillatory subsonic airflows. This later can be established by Eq. (2) and solved by using a parabolic (Rodden et al.,1971a) or quartic (Rodden et al.,1971b) approximation functions.

$$K=\left(\frac{K_1T_1}{r^2}+\frac{K_2T_2}{r^4}\right)\exp\left(-\frac{i\omega x_0}{U_\infty}\right) \tag{2}$$

In Eq. (2), ω is the actual frequency, x_0 is the distance between the sending (se) and receiving (re) points parallel to the freestream of speed of, U_∞ , $r^2=z_0^2+y_0^2$, where y_0 and z_0 are the cartesian distances between the sending and receiving points, respectively, $T_2=(z_0\cos\gamma_{re}-y_0\sin\gamma_{re})(z_0\cos\gamma_{se}-y_0\sin\gamma_{se})$, $T_1=\cos(\gamma_{re}-\gamma_{se})$, where γ_{re} and γ_{se} designates the dihedral angles of the receiving and sending points, respectively, as illustrated in Fig. 1.

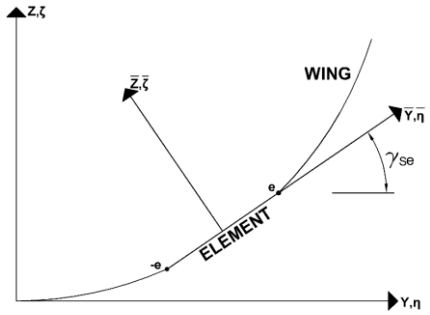

Figure 1 – The global and local coordinate systems.

The planar and nonplanar contributions of the kernel are given, respectively, as:

$$K_1 = I_1\left(u_1,k\right) + \frac{Mr}{R}\frac{\exp\left(-iku_1\right)}{\sqrt{1+u_1^2}} \tag{3.a}$$

$$K_2 = -3I_2\left(u_1,k\right) - \frac{ikM^2r^2}{R^2}\frac{\exp\left(-iku_1\right)}{\sqrt{1+u_1^2}} - \frac{Mr}{R}\left[2+\left(1+u_1^2\right)\frac{\beta^2r^2}{R^2}+\frac{Mru_1}{R}\right]\frac{\exp\left(-iku_1\right)}{\left(1+u_1^2\right)^{3/2}} \tag{3.b}$$

where M is the Mach number, $\beta=\sqrt{1-M^2}$, $u_1=\frac{MR-x_0}{\beta^2 r}$, $R=\sqrt{x_0^2+\beta^2r^2}$ and $k=\left(\omega r\right)/U_\infty$ is the reduced frequency. Based on the developments made by (Rodden et al.,1972), I_1 and I_2 are given as:

$$I_1\left(u_1,k\right) = \exp\left(-iku_1\right)\left[1-\frac{u_1}{\sqrt{1+u_1^2}} - ikI_0\left(u_1,k\right)\right] \tag{4.a}$$

$$I_2\left(u_1,k\right) = \frac{\exp\left(-iku_1\right)}{3}\left[\left(2+iku_1\right)\left(1-\frac{u_1}{\sqrt{1+u_1^2}}\right) - \frac{u_1}{\left(1+u_1^2\right)^{3/2}} - ikI_0 + k^2J_0\right] \tag{4.b}$$

For $u \geq 0$, the integrals I_0 and J_0 can be evaluated by using an approximation of, $u\left(1+u^2\right)^{-1/2}$, as proposed by Laschka (1967). It results in the following relations:

$$I_0\left(u_1,k\right) = \sum_{n=1}^{11}\frac{a_n\exp\left(-ncu_1\right)}{n^2c^2+k^2}\left(nc-ik\right) \tag{5.a}$$

$$J_0\left(u_1,k\right) = \sum_{n=1}^{11}\frac{a_n\exp\left(-ncu_1\right)}{\left(n^2c^2+k^2\right)^2}\left\{\left(n^2c^2-k^2\right)+ncu_1\left(n^2c^2+k^2\right)-ik\left[2nc+u_1\left(n^2c^2+k^2\right)\right]\right\} \tag{5.b}$$

where $c=0.372$ and the coefficients of Laschka, a_n , are given in Tab. 1.

Table 1 – Coefficients of Laschka's approximation.

n	a_n
1	0.24186198
2	–2.7918027
3	24.991079
4	–111.59196
5	271.43549
6	–305.75288
7	–41.183630
8	545.98537
9	–644.78155
10	328.72755
11	–64.279511

Otherwise, for $u < 0$, and based on the symmetry, I_1 and I_2 are given as:

$$I_1(u_1,k) = 2\,\mathrm{Re}\left[I_1(0,k)\right] - \mathrm{Re}\left[I_1(-u_1,k)\right] + i\,\mathrm{Im}\left[I_1(-u_1,k)\right] \tag{6.a}$$

$$I_2(u_1,k) = 2\,\mathrm{Re}\left[I_2(0,k)\right] - \mathrm{Re}\left[I_2(-u_1,k)\right] + i\,\mathrm{Im}\left[I_2(-u_1,k)\right] \tag{6.b}$$

At $\omega \to 0$, the planar and nonplanar parts of the kernel are computed as:

$$K_{10} = \lim_{\omega\to 0} K_1 = 1 + \frac{x_0}{R}, \quad K_{20} = \lim_{\omega\to 0} K_2 = -2 - \frac{x_0}{R}\left(2 + \frac{\beta^2 r^2}{R^2}\right) \tag{7}$$

In the DLM, it is assumed that the lifting pressure could be concentrated in a line located at the 1/4 chord line of the element and the surface boundary condition is a prescribed normalwash at the control point of each box, which is located at the 3/4 chord point along the centerline of each box, as illustrated in Fig. 2.

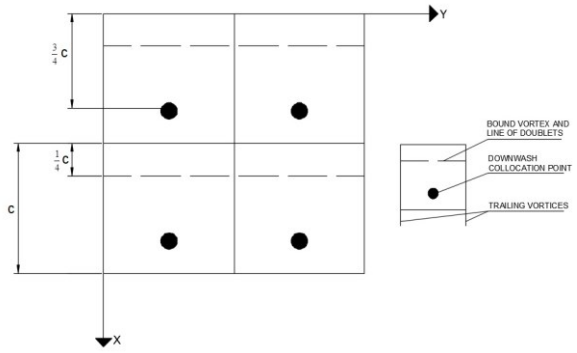

Figure 2 – Lifting surface of the aerodynamic panels to DLM.

At this time, Eq. (1) can be rewritten in the following numerical form:

$$\boldsymbol{w} = \boldsymbol{D}_{rese}\boldsymbol{p} \tag{8}$$

Where $\boldsymbol{D}_{rese}$ is the elements of the normalwash factor matrix for denoting the receiving (re) and sending(se) points.

$$\boldsymbol{D}_{rese} = \frac{\Delta x_{se}}{8\pi}\int_{-e}^{e}\left(\frac{K_1 T_1}{r^2} + \frac{K_2 T_2}{r^4}\right)\exp\left[\frac{-i\omega\left(x_0 - \bar{\eta}\tan\lambda_{se}\right)}{U_\infty}\right]d\bar{\eta} \tag{9}$$

By evaluating the normalwash factor in Eq. (8) by adding and subtracting the steady values of K_1 and K_2, denoted by K_{10} and K_{20}, Eq. (9) can be written as:

$$\boldsymbol{D}_{rese} = \boldsymbol{D}_{0rese} + \boldsymbol{D}_{1rese} + \boldsymbol{D}_{2rese} \tag{10}$$

where the components related to the steady, planar and nonplanar unsteady are given, respectively, as follow, $\boldsymbol{D}_{0rese} = \frac{\Delta x_s}{8\pi}\int_{-e}^{e}\left(\frac{K_{10}T_1}{r^2} + \frac{K_{20}T_2}{r^4}\right)d\bar{\eta}$, $\boldsymbol{D}_{1rese} = \frac{\Delta x_s}{8\pi}\int_{-e}^{e}\frac{Q_1(\bar{\eta})}{r^2}d\bar{\eta}$ and $\boldsymbol{D}_{2rese} = \frac{\Delta x_s}{8\pi}\int_{-e}^{e}\frac{Q_2(\bar{\eta})}{r^4}d\bar{\eta}$, and the aerodynamic influence coefficients matrix (AIC) is defined as, $\boldsymbol{AIC} = \boldsymbol{D}_{rese}^{-1}$.

Now, it is necessary to estimate the incremental oscillatory normalwash factor by performing an interpolation of the numerators as quartics form, such as:

$$Q_1(\bar{\eta}) = A_1\bar{\eta}^2 + B_1\bar{\eta} + C_1 + D_1\bar{\eta}^3 + E_1\bar{\eta}^4 \cong K_1T_1\exp\left[\frac{-i\omega\left(x_0 - \bar{\eta}\tan\lambda_{se}\right)}{U_\infty}\right] - K_{10}T_1 \tag{11.a}$$

$$Q_2(\bar{\eta}) = A_2\bar{\eta}^2 + B_2\bar{\eta} + C_2 + D_2\bar{\eta}^3 + E_2\bar{\eta}^4 \cong K_2T_2\exp\left[\frac{-i\omega\left(x_0 - \bar{\eta}\tan\lambda_{se}\right)}{U_\infty}\right] - K_{20}T_2 \tag{11.b}$$

It must be emphasized that, the inboard, inboard intermediate, center, outboard intermediate and outboard values of $Q_1(\bar{\eta})$ along a line of the lifting pressure are given by the relations, $Q_1(-e)$, $Q_1(-e/2)$, $Q_1(0)$, $Q_1(e/2)$ and $Q_1(e)$, respectively. Thus, the coefficients appearing in Eqs. (11) are defined as:

$$A_1 = -\frac{1}{6e^2}\left[Q_1(-e) - 16Q_1(-e/2) + 30Q_1(0) - 16Q_1(e/2) + Q_1(e)\right] \tag{12.a}$$

$$B_1 = \frac{1}{6e}\left[Q_1(-e) - 8Q_1(-e/2) + 8Q_1(e/2) - Q_1(e)\right] \tag{12.b}$$

$$C_1 = Q_1(0) \tag{12.c}$$

$$D_1 = -\frac{2}{3e^3}\left[Q_1(-e) - 2Q_1(-e/2) + 2Q_1(e/2) - Q_1(e)\right] \tag{12.d}$$

$$E_1 = \frac{2}{3e^4}\left[Q_1(-e) - 4Q_1(-e/2) + 6Q_1(0) - 4Q_1(e/2) + Q_1(e)\right] \tag{12.e}$$

By performing the same procedure for $Q_2(\bar{\eta})$, the planar downwash factor is:

$$\begin{aligned} \boldsymbol{D}_{1rese} = \frac{\Delta x_{se}}{8\pi}\Big\{&\Big[\left(\bar{y}^2 - \bar{z}^2\right)A_1 + \bar{y}B_1 + C_1 + \bar{y}\left(\bar{y}^2 - 3\bar{z}^2\right)D_1 + \left(\bar{y}^4 - 6\bar{y}^2\bar{z}^2 + \bar{z}^4\right)E_1\Big]F + \\ &\ldots\left[\bar{y}A_1 + \frac{1}{2}B_1 + \frac{1}{2}\left(3\bar{y}^2 - \bar{z}^2\right)D_1 + 2\bar{y}\left(\bar{y}^2 - \bar{z}^2\right)E_1\right]\log\frac{(\bar{y}-e)^2 + \bar{z}^2}{(\bar{y}+e)^2 + \bar{z}^2} + \\ &\ldots 2e\left[A_1 + 2\bar{y}D_1 + \left(3\bar{y}^2 - \bar{z}^2 + \frac{1}{3}e^2\right)E_1\right]\Big\} \end{aligned} \tag{13}$$

where $\varepsilon = \dfrac{e^2}{\bar{z}^2}\left[1 - \dfrac{\bar{y}^2 + \bar{z}^2 - e^2}{2e|\bar{z}|}\,atan\left(\dfrac{2e|\bar{z}|}{\bar{y}^2 + \bar{z}^2 - e^2}\right)\right]$ and $F = \dfrac{2e\delta_1}{\bar{y}^2 + \bar{z}^2 - e^2}\left(1 - \varepsilon\dfrac{\bar{z}^2}{e^2}\right) + \dfrac{\pi\delta_2}{|\bar{z}|}$.

Thus, for the general case, the nonplanar downwash factor is given as:

$$\begin{aligned} \boldsymbol{D}_{2rese} = \frac{e\Delta x_{se}}{8\pi(\bar{y}^2 + \bar{z}^2 - e^2)}\Bigg\{&\frac{1}{\left[(\bar{y}+e)^2 + \bar{z}^2\right]\left[\left[(\bar{y}-e)^2 + \bar{z}^2\right]\right]}[2\left(\bar{y}^2 + \bar{z}^2 + e^2\right)\left(e^2A_2 + C_2\right) + \\ &\ldots 4\bar{y}e^2B_2 + 2\bar{y}\left(\bar{y}^4 - 2e^2\bar{y}^2 + 2\bar{y}^2\bar{z}^2 + 3e^4 + 2e^2\bar{z}^2 + \bar{z}^4\right)D_2 + \\ &\ldots 2\left(3\bar{y}^6 - 7e^2\bar{y}^4 + 5\bar{y}^4\bar{z}^2 + 6e^4\bar{y}^2 + 6e^2\bar{y}^2\bar{z}^2 - 3e^2\bar{z}^4 - \bar{z}^6 + \bar{y}^2\bar{z}^4 - 2e^4\bar{z}^2\right)E_2] - \\ &\ldots\frac{(\delta_1\varepsilon + \Gamma)}{e^2}\left[\left(\bar{y}^2 + \bar{z}^2\right)A_2 + \bar{y}B_2 + C_2 + \bar{y}\left(\bar{y}^2 + 3\bar{z}^2\right)D_2 + \left(\bar{y}^4 + 6\bar{y}^2\bar{z}^2 - 3\bar{z}^4\right)E_2\right]\Big\} + \\ &\ldots\frac{\Delta x_{se}}{8\pi}\left\{\frac{D_2}{2}\log\frac{(\bar{y}-e)^2 + \bar{z}^2}{(\bar{y}+e)^2 + \bar{z}^2} + 2\left[e + \bar{y}\log\frac{(\bar{y}-e)^2 + \bar{z}^2}{(\bar{y}+e)^2 + \bar{z}^2}\right]E_2\right\} \end{aligned} \tag{14}$$

where $\Gamma = \dfrac{e^2}{|\bar{z}|^2}\left[1 - \delta_1 - \dfrac{\delta_2\pi}{|\bar{z}|}\left(\dfrac{\bar{y}^2 + \bar{z}^2 - e^2}{2e}\right)\right]$, $(\delta_1, \delta_2) = (1,0)$ for $\bar{y}^2 + \bar{z}^2 - e^2 > 0$, $(\delta_1, \delta_2) = (1, 0.5)$ for $\bar{y}^2 + \bar{z}^2 - e^2 = 0$ and $(\delta_1, \delta_2) = (1,1)$ for $\bar{y}^2 + \bar{z}^2 - e^2 < 0$.

3. FE MODELING OF THE VISCOELASTIC SANDWICH STRUCTURE

3.1 Complex modulus approach

It is proposed herein the use of the complex modulus with the Frequency and Temperature Superposition Principle (FTSP) (Nashif,1985) to characterize the viscoelastic damping mechanism of the aeroviscoelastic system under subsonic airflows.

According to the linear viscoelastic theory and the FTSP, the complex modulus approach of viscoelastic materials is given as:

$$G(\alpha_T\omega, T) = G'(\alpha_T\omega, T) + iG''(\alpha_T\omega, T) \tag{15.a}$$

or,

$$G(\alpha_T\omega,T)=G'(\alpha_T\omega,T)\left[1+i\eta(\alpha_T\omega,T)\right] \tag{15.b}$$

where $G'(\alpha_T\omega,T)$, $G''(\alpha_T\omega,T)$ and $\eta(\alpha_T\omega,T)=G''(\alpha_T\omega,T)/G'(\alpha_T\omega,T)$ are known as storage and loss moduli and loss factor, respectively, ω is the excitation frequency, T is the operating temperature, and a_T is the shift factor, which is a function of the temperature.

Drake and Soovere (1984) have proposed analytical expressions for the complex modulus and shift factor for various viscoelastic materials frequently used in practical applications. For example, for the 3M ISD112TM material adopted in this study, they have suggested the following complex modulus and shift factor relations, valid for the temperature and frequency intervals of $210 \le T \le 360K$ and $1.0 \le \omega \le 1.0\times10^6\ Hz$:

$$G(\omega,T)=0.4307+\frac{1200}{1+3.241\times\left(\frac{i\omega\alpha_T}{1543000}\right)^{-0.18}+\left(\frac{i\omega\alpha_T}{1543000}\right)^{-0.6847}}\ [MPa] \tag{16}$$

where $\alpha_T=10^{\left(-3758.4\times\left(\frac{1}{T}-0.00345\right)-225.06\times\log(0.00345\times T)+0.23273\times(T-290)\right)}$, T is the temperature in Kelvin, ω is the frequency in rad/s and G is the complex modulus in N/m^2.

3.2 Three-layer sandwich plate element

In this section, the FE modeling of the sandwich plate element used in this study, as depicted in Fig. 3, is summarized. It is composed by a base-plate (1), a viscoelastic core (2) and a constraining layer (3), and four nodes and seven degrees of freedom (DOFs) per node: the longitudinal displacements u and v in directions x and y, respectively, for the face layers; the transverse displacement, w; and the rotations, $\theta_x=\partial w/\partial y$ and $\theta_y=\partial w/\partial x$.

To develop the theory, the materials are considered isotropic and homogeneous with linear behavior. For the face elastic layers, it is used the Kirchhoff's hypothesis, and the Mindlin's hypothesis is assumed for the viscoelastic part with the aim of accounting for the transverse shear strains.

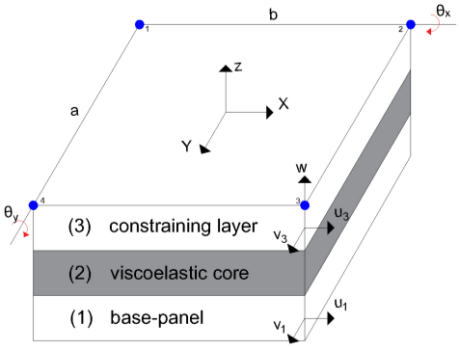

Figure 3 – Illustration of the three-layer sandwich plate element.

The discretization within the sandwich plate element is done by using the general relation, $\boldsymbol{u}(x,y,t)=\boldsymbol{N}(x,y)\boldsymbol{u}_{(e)}(t)$, where matrix $\boldsymbol{N}(x,y)$ contains the linear and cubic shape functions used to approximate the longitudinal and transverse displacements, respectively, and vector $\boldsymbol{u}_{(e)}(t)=\left[u_1^i\ v_1^i\ u_3^i\ v_3^i\ w^i\ \theta_x^i\ \theta_y^i\right]^T$ contains the nodal DOFs, with $i=1$ to 4. The strain-displacement relations can be given as, $\boldsymbol{\varepsilon}(x,y,z,t)=\boldsymbol{B}(x,y,z)\boldsymbol{u}_{(e)}(t)$, where the strains for the elastic and viscoelastic layers are, $\boldsymbol{\varepsilon}_k=\left[\varepsilon_x^{(k)}\ \varepsilon_y^{(k)}\ \gamma_{xy}^{(k)}\right]^T$ and $\boldsymbol{\varepsilon}_2=\left[\varepsilon_x^{(2)}\ \varepsilon_y^{(2)}\ \gamma_{xy}^{(2)}\ \gamma_{xz}^{(2)}\ \gamma_{yz}^{(2)}\right]^T$, respectively, with $(k=1,3)$.

Based on the stress-strain state for each layer, the corresponding stress response, $\boldsymbol{s}(x,y,z,t)=\boldsymbol{C}\,\boldsymbol{B}(x,y,z)\boldsymbol{u}_{(e)}(t)$, can be found, where $\boldsymbol{C}=\boldsymbol{C}_k$ is the material properties matrix related to the elastic layers, and matrix $\boldsymbol{C}=\boldsymbol{C}_2(\omega,T)$ contains the temperature- and frequency-dependent mechanical properties of the viscoelastic core. The differential operators of the

strain-displacements relations are given in matrix, $\boldsymbol{B}(x,y,z)$. Details of these developments can be found in (Lima et al., 2009, 2010).

After applying the variational principles to define the kinetic and strain energies of each layer, the following elementary FE mass and stiffnesses matrices can be found:

$$\boldsymbol{M}^{(e)} = \sum_{k=1}^{3} \rho_k h_k \int_{x=0}^{b} \int_{y=0}^{a} \boldsymbol{N}^T(x,y)\boldsymbol{N}(x,y)dydx \tag{17.a}$$

$$\boldsymbol{K}_e^{(e)} = \sum_{k=1,3} \int_{z=0}^{h_k} \int_{x=0}^{b} \int_{y=0}^{a} \boldsymbol{B}_k^T(x,y,z)\boldsymbol{C}_k\boldsymbol{B}_k(x,y,z)dydxdz \tag{17.b}$$

$$\boldsymbol{K}_v^{(e)}(\omega,T) = \int_{z=0}^{h_v} \int_{x=0}^{b} \int_{y=0}^{a} \boldsymbol{B}_2^T(x,y,z)\boldsymbol{C}_2(\omega,T)\boldsymbol{B}_2(x,y,z)dydxdz \tag{17.c}$$

where h_k and ρ_k are the thickness and mass density of layer k , respectively, b and a are the dimensions of the element y and x directions, respectively $\boldsymbol{K}_e^{(e)} = \boldsymbol{K}_1^{(e)} + \boldsymbol{K}_3^{(e)}$ and $\boldsymbol{K}_v^{(e)}(\omega,T) = \boldsymbol{K}_2^{(e)}(\omega,T)$ represent the stiffnesses of the elastic and viscoelastic parts.

By assembling the elementary matrices for a given FE mesh with N DOFs and considering the following relation between the complex shear and longitudinal *moduli* of the viscoelastic material, $G(\omega,T) = E(\omega,T)/2(1+\nu)$, for a frequency-and temperature-independent Poisson ratio, it is possible to obtain the following equations of motion:

$$\boldsymbol{F}(\omega) = \boldsymbol{Z}(\omega,T)\boldsymbol{U}(\omega,T) \tag{18}$$

where $\boldsymbol{Z}(\omega,T) = \boldsymbol{K}_e + G(\omega,T)\overline{\boldsymbol{K}}_v - \omega^2\boldsymbol{M}$ is the complex frequency- and temperature-dependent dynamic stiffness matrix, with $\boldsymbol{M}, \boldsymbol{K}_e, \overline{\boldsymbol{K}}_v \in R^{NxN}$, $\boldsymbol{U}(\omega,T) \in R^{NxN}$ and $\boldsymbol{F}(\omega) \in R^{NxN}$ are the vectors of nodal displacements and external forces, respectively.

4. FORMULATING THE AEROVISCOELASTIC PROBLEM

In this section, the structural and aerodynamic models will be coupled to generate the aeroviscoelastic problem for flutter predictions. The coupling between the structural displacements and aerodynamic panels is done by using splines interpolation functions, where the structural deformations of the middle plane of the sandwich structure are approximated through polynomials in the plane directions, as discussed in (Blair, 1994) and (Kotikalpudi, 2015). Within this aim, it is considered the equation of motion of the viscoelastically damped structure in the modal domain as follows:

$$\boldsymbol{F}_{\mathrm{m}} = \boldsymbol{Z}_m(\omega,T)\boldsymbol{\eta}(\omega,T) \tag{19}$$

where $\boldsymbol{F}_m$ and $\boldsymbol{\eta}(\omega,T)$ are the external forces and displacements of the system in the modal domain, respectively. In this case, the nodal deformations for a given mode of vibration, ϕ_j , is given by the relation, $\boldsymbol{\delta}(\omega,T) = \sum_{j=1}^{m} \phi_j \boldsymbol{\eta}(\omega,T)$.

In the following developments, the frequency- and temperature-dependent terms will be omitted in order to simply the mathematical notation.

Based on the nDLM method (Kotikalpudi, 2015), the loading acting on the control point of an aerodynamic panel can be computed using the $\boldsymbol{AIC}$ as:

$$\boldsymbol{F}_a = q_\infty \boldsymbol{SwAICh} \tag{20}$$

where $q_\infty = 0.5\rho_{air}U_\infty^2$ is the dynamic pressure, ρ_{air} is the air density, U_∞ is the airspeed, $\boldsymbol{h}$ contains the nodal displacements at the control point of the panels and $\boldsymbol{S}$ is the surface area.

By considering the polynomial interpolation of the structural nodal displacements given by $\boldsymbol{T}_{spline}$ at 3/4 of the chord line in the aerodynamic mesh, the connection between the aerodynamic and structural meshes can be obtained by the relation, $\boldsymbol{T}_{as} = \boldsymbol{T}_{\mathrm{int}}\boldsymbol{T}_{spline}$, where $\boldsymbol{T}_{\mathrm{int}}(x,y) = \sum_{j=0}^{nx}\sum_{k=0}^{ny} \boldsymbol{x}^j\boldsymbol{y}^k$ represents the nodal deformations. Therefore, it is possible to compute the downwash, $w = \dfrac{\partial \boldsymbol{h}}{\partial t} + U_\infty \dfrac{\partial \boldsymbol{h}}{\partial x}$, in such a way that, $\boldsymbol{h} = \boldsymbol{T}_{as}$ (Blair,1994).

In order to understand the connection between the structural and aerodynamic meshes, a surface with four panels is illustrated in Fig 4.

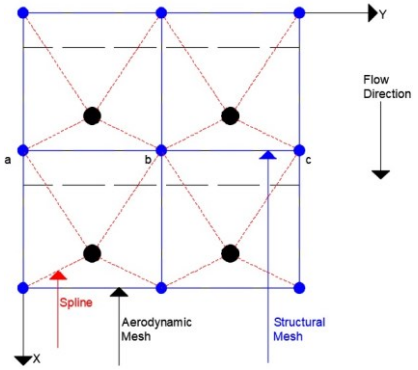

Figure 4 – Interpolation of the control point for the aerodynamic mesh using the nodal deformations of the structural mesh.

Thus, based on the transformation matrix, $\boldsymbol{T}_{as}$, it is possible to obtain the relation, $\boldsymbol{F}_{\mathrm{m}} = \phi \boldsymbol{T}_{as}^{T} \boldsymbol{T}_{aero}$, which enables to obtain the distribution of the aerodynamic loadings acting on the viscoelastic structure as, $\boldsymbol{F}_{\mathrm{m}} = q_{\infty} \boldsymbol{Q} \boldsymbol{\eta}$. It enables to establish the following expression for the GAM matrix:

$$\boldsymbol{Q} = \phi^{T} \boldsymbol{T}_{as}^{T} \boldsymbol{S} \boldsymbol{w} \boldsymbol{A} \boldsymbol{I} \boldsymbol{C} \boldsymbol{T}_{as} \boldsymbol{h} \phi \tag{21}$$

where matrix GAM is dependent of the Mack number, reduced frequency and operating temperature of the aeroviscoelastic system.

Hence, by combining Eq. (19) with, $\boldsymbol{F}_{\mathrm{m}} = q_{\infty} \boldsymbol{Q} \boldsymbol{\eta}$, the resulting eigenvalue problem, $\boldsymbol{Z}_{m}(\omega, T)\boldsymbol{\eta} = 0.5 \rho_{air} U_{\infty}^{2} \boldsymbol{Q} \boldsymbol{\eta}$, to evaluate the stability of the system based on the assumption that, it is unstable if the imaginary part of a given eigenvalue becomes positive. However, due to the presence of the viscoelastic part, the GAM matrix is complex and frequency- and temperature-dependent. Clearly, it makes the stability analysis of the system more complicated since the reduced frequency is dependent on the natural frequencies to be computed. It means that the complex eigenvalue problem to be solved is nonlinear. To overcome this drawback, it is proposed herein a modification of the classical pk method (Hassig, 1971) based on the introduction of an iterative procedure for the aeroviscoelastic problems to compute their eigenvalues and eigenvectors for the purposes of flutter boundary predictions.

5. THE ROGER'S APPROXIMATION

Taking into account the fact that, the aerodynamic forces are computed for a given set of reduced frequencies, $k = \omega b / U_{\infty}$, and the Mach number, which are transformed to the time domain by means of a transfer function and polynomial expressions using the Laplace variable, $s = i\omega$, with, $ik = s\left(b/U_{\infty}\right)$. In this approach, Eq. (21) for the GAM matrix is approximated by Eq. (22) using the so-called Roger's terms $[A_0, \ldots, A_m]$, (Roger,1977):

$$\boldsymbol{Q}(k) = A_0 + A_1 \left(\frac{b}{U_{\infty}}\right) s + A_2 \left(\frac{b}{U_{\infty}}\right)^{2} s^{2} + \sum_{m=3}^{6} \frac{A_m s}{\left(s + U_{\infty} \beta_{m-2} / b\right)} \tag{22}$$

where $\beta_{m-2} = -1.7 k_{\max} \dfrac{n}{(n+1)^{2}}$ is obtained empirically for a given reduced frequency, k_n , with $k_{\max}$ the maximum value of the reduced frequency.

6. THE MODIFIED PK METHOD

In this study, it is used a modified version of the pk method with the aim of computing the complex eigenvalues and eigenvectors of the resulting aeroviscoelastic system. Based on the developments made by Rodden and Johnson (1994), the complex eigenvalue problem to be solved can be established as follows:

$$\left| p^2 \boldsymbol{I} + \boldsymbol{M}^{-1}\left[\boldsymbol{K}_e + G(\omega,T)\bar{\boldsymbol{K}}_v - \frac{\rho_{air}U_\infty^2}{2}\boldsymbol{Q} \right] \right| = \boldsymbol{0} \tag{22}$$

Another alternative, is to rewritten Eq. (23) in the following state-space form, $[\boldsymbol{A} - p\boldsymbol{I}]\boldsymbol{\eta} = 0$, where, for the present problem, the state matrix is given as:

$$\boldsymbol{A} = \begin{bmatrix} \boldsymbol{0} & \boldsymbol{I} \\ -\boldsymbol{M}^{-1}\left[\boldsymbol{K}_e + G(\omega,T)\bar{\boldsymbol{K}}_v - \frac{\rho_{air}U_\infty^2}{2}\mathrm{Re}(\boldsymbol{Q}) \right] & -\boldsymbol{M}^{-1}\left[-\frac{\rho_{air}bU_\infty}{4k}\mathrm{Im}(\boldsymbol{Q}) \right] \end{bmatrix} \tag{23}$$

Thus, for an iteration, j, and for a given temperature, the resolution of Eq. (24) results in complex pairs of eigenvalues, $p = \omega\left(\frac{g}{2} \pm i\right)$, where $\omega = \mathrm{Im}(p)$ is the natural frequency and $g = \frac{2\mathrm{Re}(p)}{\mathrm{Im}(p)}$ is the damping parameter. In this study, at each iteration, j, on the airspeed, it is used a convergence based on the reduced frequency, $\left|k^{(j)} - k^{(j-1)}\right| < \varepsilon$ for $k^{(j-1)} < 1$ and $\left|k^{(j)} - k^{(j-1)}\right| < \varepsilon k^{(j-1)}$ for $k^{(j-1)} \geq 1$, where $\varepsilon = 0.001$ is the tolerance that has been adopted in the simulations.

7. NUMERICAL APPLICATIONS AND DISCUSSIONS

7.1 Stability analysis of the curved panel without passive CVLs

The current analysis employs an untreated curved panel as depicted in Fig. 5, characterized by specific physical and geometric properties: elastic modulus, $210\times10^9\ N/m^2$; Poisson's ratio, 0.3; panel thickness, $1.5mm$; mass density, $7800\ kg/m^3$; chord length, $720mm$; radius of curvature, $938mm$; and curvature angle, $\varphi = 41.5°$. The primary objective here is to assess the first five natural frequencies of the system without utilizing passive CVLs. This evaluation is accomplished by calculating the Modal Assurance Criterion (MAC) for two scenarios: the first, regarded as the reference, involves using the SHELL63 element provided by the ANSYS® software; in the second scenario, all these elements are replaced with the base-plate element developed in this study, utilizing the in-house code AEROSOLVER.

The results, presented in Table 2 for a 6x6 mesh, illustrate the precision of the proposed interface strategy for conducting dynamic analyses of systems with more intricate geometries. Notably, the MAC values are found to be very close to 100%.

Figure 5 – Representation of the untreated curved panel.

Table 2 – Comparison between the natural frequencies of the untreated curved panel generated by the ANSYS® and AEROSOLVER.

Frequency [Hz]		MAC
ANSYS®	AEROSOLVER	
1.4375	1.4375	99.63
3.3137	3.3175	99.35
8.3987	8.3987	99.58
11.1790	11.1780	99.68
24.2540	24.2542	99.72

Additionally, in order to minimize the impact of mesh refinement on flutter boundary predictions, a convergence analysis was carried out to determine the minimum number of finite elements (FE) and panels required for structural and aerodynamic meshes to converge the natural frequencies and the initial critical flutter speed. In this context, the subsonic airflow flight conditions include: six panels in both the chord and wingspan directions, Mach number, $M = 0.25$, air density , $\rho_{air} = 1.1839 kg/m^3$, operating temperature , $T = 25°C$, and a specified reduced frequency range , $k = [0 - 3.6]$.

Table 3 presents the results of the convergence for the five natural frequencies and the first critical flutter speed of the curved panel without viscoelastic treatment. Clearly, a mesh size of 6x6 FE has proven to be sufficient in obtaining accurate results for the fifth natural frequency and the initial critical flutter speed of the aero-viscoelastic problem. Consequently, in the subsequent simulations, a 6x6 mesh will be used for both the structural and aerodynamic domains.

Table 3 – Convergence analysis for the curved panel without treatment.

Mesh	5° Natural Frequency [Hz]	1ª Flutter speed [m/s]
2x2	14.19	1
4x4	24.05	28
6x6	24.25	27
8x8	24.31	27
10x10	24.33	27
15x15	24.37	27
17x17	24.37	27

It is important to note that when conducting stability analyses in subsonic conditions, the unsteady aerodynamic forces exerted on the viscoelastically damped structure are calculated through the application of the nDLM (Nonlinear Dynamic Loads Model) within the AEROSOLVER code. In this context, a reduced frequency range is employed to derive the matrix and predict the system's flutter boundary.

In the Fig. 6 displays the aeroelastic findings in the form of Vg and Vω plots, which were employed to detect the first coalescence of the vibration modes for the aeroelastic system without viscoelastic treatment. In this scenario, simulations were conducted over an airspeed range of, $[0 - 30 m/s]$utilizing the classical pk method. It is evident that a critical flutter speed of approximately was observed, $27 m/s$, primarily induced by the second vibration mode (twist mode) of the curved panel. However, for this specific test case, the Vω diagram indicates the presence of a static divergence phenomenon for the first mode, occurring at an airspeed of, $23 m/s$, i.e., prior to the onset of the flutter phenomenon.

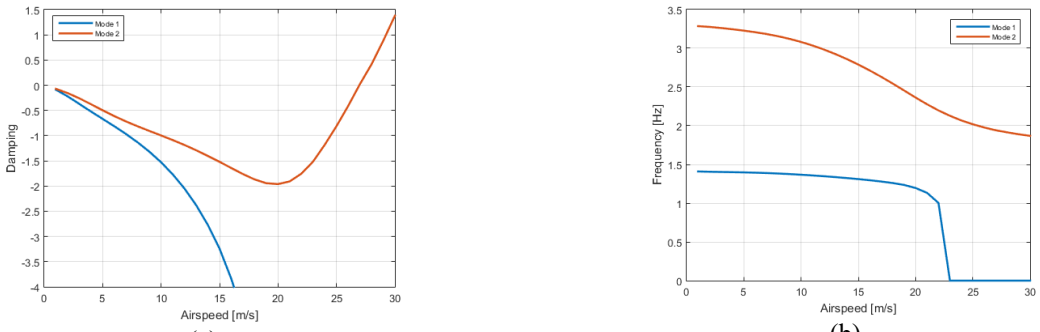

(a) (b)

Figure 6 – Vg (left) and Vω (right) diagrams of the curved panel without CVL.

7.2 Stability analysis of the curved panel with passive CVLs

In this section, it is focused on stability analysis and flutter suppression for the curved panel that has been equipped with passive CVLs. The viscoelastic material utilized in the forthcoming simulations is 3M ISD112™, characterized by a complex modulus function outlined in Eq. (16). Initially, assuming an operational temperature of, $T = 25°C$, it is assumed the complete application of passive CVLs to the panel using a 6x6 finite element mesh, as determined through the convergence analysis conducted in the preceding section.

The physical and geometrical properties of the base-panel and constraining layer are the same, as given in Section 7.1. But, the thickness of the constraining layer is of, $0.5mm$. The material properties of the viscoelastic core are: Poisson's ratio, 0.49 ; mass density, $950 kg/m^3$; thickness, $0.0254mm$.

Table 4 illustrates that incorporating the viscoelastic and constraining layers onto the base-panel results in an elevation of both its overall mass and stiffness. As anticipated, this leads to an increase in the first two natural frequencies. It's evident that, for practical applications with industrial relevance, particularly in the aerospace sector, it is prudent to employ a design approach for the application of CVLs that considers their effectiveness and limitations related to mass addition.

Table 4 – Convergence analysis for the curved panel without treatment.

Mode	Natural frequency [Hz]
1	2.6706
2	7.6635

Fig. 7 displays the outcomes of the aeroviscoelastic system within an airspeed range of, $[0-100 m/s]$.When comparing these outcomes with those presented in Fig. 6, it's evident that the presence of viscoelastic treatment leads to a noticeable increase in the flutter speed. Specifically, a critical flutter speed of, $87 m/s$,was observed in the case with viscoelastic treatment, in contrast to a critical flutter speed of, $27 m/s$ in the untreated system. Additionally, the static divergence phenomenon occurred at an airspeed of, $97 m/s$ due to the increased elastic stiffness of the base-panel. This illustrates the efficacy of surface viscoelastic treatment in subsonic flutter suppression. These results also showcase the effectiveness of the proposed modeling approach, which involves coupling between Finite Element Method (FEM) and the nDLM method, for conducting stability analyses of aeroviscoelastic systems operating in subsonic conditions.

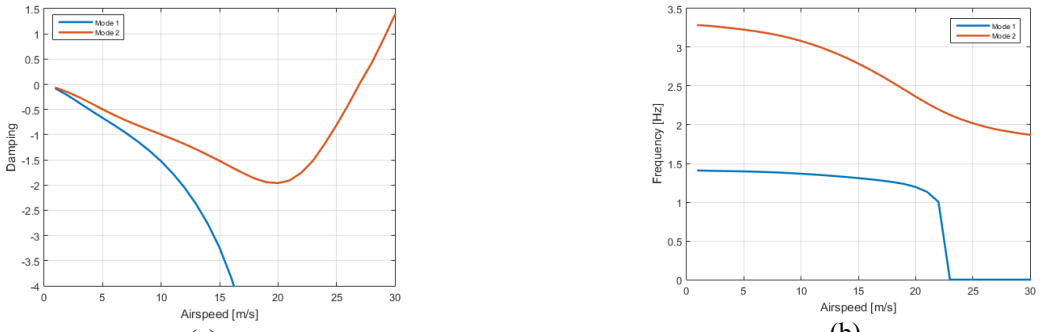

(a) (b)

Figure 7– Vg (left) and Vω (right) diagrams of the curved panel with CVL.

7.3. Influence of the operating temperature

As previously discussed, the dynamic behavior of viscoelastic materials is notably influenced by the excitation frequency and temperature. Consequently, it's expected that their damping performance in subsonic aeroelastic applications will also be impacted. Hence, it becomes crucial to explore the extent of the temperature's influence on flutter conditions.

Fig. 8 illustrates the impact of operating temperature on the critical flutter speed of the aero-viscoelastic system. It's evident that, as temperature increases, there is a significant decrease in the flutter speed. This can be attributed to a decrease in the loss factor (damping capacity) of the viscoelastic material.

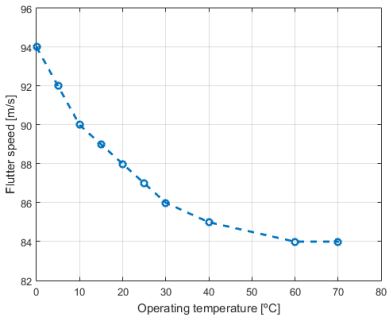

Figure 12 – Influence of the temperature on the flutter boundary of the panel with CVL.

8. CONCLUSIONS

In this study, a numerical modeling methodology that combines Finite Element Method (FEM) with the nDLM for stability analyses of aeroviscoelastic systems under subsonic airflows. Additionally, has been proposed an interface strategy between our in-house code, AEROSOLVER, and the commercially available ANSYS® code for applications involving more complex systems in terms of geometry and degrees of freedom (DOFs).

Analyzing the results of simulations for curved panels with and without viscoelastic treatment, it can conclude that this type of control, commonly used for mitigating vibration and noise, can also effectively address aeroelastic instability induced by subsonic flutter phenomena. It represents a valuable control alternative for enhancing aeroelastic stability in existing or new structures, offering the advantage of cost-effective application and maintenance when compared to active and semi-active control strategies.

However, it's important to note that the aeroelastic response of systems with viscoelastic materials is significantly affected by operating temperature and geometric parameters. For example, it has been observed that as the operating temperature increases, the flutter boundary decreases substantially. This reduction is attributed to the diminished damping capacity of the viscoelastic component at higher temperature levels.

9. ACKNOWLEDGEMENTS

The authors are grateful to CNPq and FAPEMIG for the continued support to their research activities through the research Grants 306138/2019-0 and PPM-0058 (A.M.G. de Lima), respectively, as well as the CAPES foundation for the PhD grants.

10. REFERENCES

Bagley, R.L., Torvik, P.J.,1985. A. Fractional calculus in the transient analysis of viscoelastically damped structures, The Am. Institute of Aeronautics and Astronautics J., Vol. 23, pp. 918-925. https://doi.org/10.2514/3.9007

Bismarck-Nasr, M.N., Kernel function occurring in subsonic unsteady potential flow, AIAA J., Vol. 29, pp. 878–879. https://doi.org/10.2514/3.10673

Blair, M., 1994. A compilation of the mathematics leading to the doublet-lattice method, Air Force Wright Aeronautical Laboratories, Wright-Patterson Air Force Base, Ohio, WL-TR-95-3022.

Botez, R.M., Doin, A., Biskri, D.E., Cotoi, I., Hamza, D., Parvu, P., 2003. Method for flutter aero-servoelastic open loop analysis, Canadian Aeronautics and Sp. J., Vol. 49, pp. 179-190. https://doi.org/10.1115/IMECE2002-33623

Brendel, M., Sulaeman, E., 1994. Improved doublet lattice formulation for calculating aerodynamic loads on lifting surfaces in unsteady subsonic flow, 12th Appl. Aerodynamics Conf. https://doi.org/10.2514/6.1994-1890

Cunha, B.S.C., de Lima, A.M.G., Silva, A.R., Rodovalho, L.F.F., 2017. Vortex-induced vibration analysis of viscoelastically mounted rigid circular cylinders in cross-flow at a moderate Reynolds number, J. of Vib. and Control., Vol. 24, pp. 2688–2700. https://doi:10.1177/107754631773365

Cunha-filho, A.G., de Lima, A.M.G., Donadon, M.V., Leão, L.S., 2019. Flutter suppression of plates using passive constrained viscoelastic layers, Mech. Systems and Signal Process., Vol. 79, pp. 99-111. https://doi.org/10.1016/j.ymssp.2016.02.025

De Lima, A.M.G., Faria, A.W., Rade, D.A., 2010. Sensitivity analysis of frequency response functions of composite sandwich plates containing viscoelastic layers, Compos. Struct., Vol. 92, pp. 364-376. https://doi.org/10.1016/j.compstruct.2009.08.017

Drake, M.L., Soovere, J., 1984. A design guide for damping of aerospace structures, In: 3th AFWAL Vib. Damping Workshop Proc.

De Lima, A.M.G., Rade, D.A., Lépore-neto, F.P., 2009. An efficient modeling methodology of structural systems containing viscoelastic dampers based on frequency response function substructuring, Mech. Systems and Signal Process., Vol. 23, pp. 1272–1281. https://doi.org/10.1016/j.ymssp.2008.09.005

Galucio, A.C., Deü, J.F., Ohayon, R. ,2004. Finite element formulation of viscoelastic sandwich beams using fractional derivative operators, Computational Mech., Vol. 33, pp. 282-291. https://doi.org/10.1007/s00466-003-0529-x

Hassig, H.J., 1971. An approximate true damping solution of the flutter equation by determinate iteration, J. of Aircr., Vol. 8, pp. 885-889. https://doi.org/10.2514/3.44311

Ingram, C.W., Szwarc, W.J., 1976. Passive flutter suppression, J. of Aircr., Vol. 13, pp. 542-543. https://doi.org/10.2514/3.44544

Kotikalpudi, A., Pfiper, H., Balas, G.J., 2015. Unsteady aerodynamics modeling for a flexible unmanned air vehicle, AIAA Atmospheric Flight Mech. Conf., Dallas, TX. https://doi.org/10.2514/6.2015-2854

Laschka, B., 1967. The pressure, lift and moment distributions on a harmonically oscillating sweptback wing of low aspect ratio at low subsonic speeds; comparison between theory and measurements, Proc. of International Counc. of the Aeronautical Sci., 4th Congress, Paris, pp. 295-313.

Lighthill, M., 1953. Oscillating airfoils at high mach number, J. of Aeronautical Sci., Vol. 20, pp. 402-406. https://doi.org/10.2514/8.2657

Nashif, A.D., Jones, D.I.G., Handerson, J.P., 1985. Vibration Damping, John Wiley and Sons New York, USA.

Merrett, C.G., Hilton, H.H.,2010. Elastic and viscoelastic panel flutter in incompressible, subsonic and compressible flows, ASD J., Vol. 2, pp. 53-80.

Moon, S.H., Kim, S.J., 20101. Active and passive suppressions of nonlinear panel flutter using finite element method, AIAA J., Vol. 39, pp. 2042-2050. https://doi.org/10.2514/2.1217

Rodden, W.P., Giesing, J.P., Kalman, T.P., 1971a .New developments and applications of the subsonic doublet-lattice method for nonplanar configurations, AGARD Conf. Proc., Part II, CP-80-71. https://doi.org/10.2514/3.59117

Rodden, W.P., Giesing, J.P., Kalman, T.P., 1971b. Subsonic unsteady aerodynamics for general configurations, Air Force Wright Aeronautical Laboratories, Wright-Patterson Air Force Base, Ohio, Part. I, AFFDL-TR-71-5. https://doi.org/10.2514/6.1972-26

Rodden, W.P., Giesing, J.P., Kalman, T.P., 1972. Refinement of the nonplanar aspects of the subsonic doublet-lattice lifting surface method, J. of Aircr., Vol. 9, pp. 69-73. https://doi.org/10.2514/3.44322

Rodden, W.P., Johnson, E.H., 1994. MSC/NASTRAN handbook for aeroelastic analysis, Vol. 68, MacNeal-Schwendler Corp., Los Angeles, CA.

Rodden, W.P., Taylor, P.F., Mcintosh, S.C., 1998. Further refinement of the subsonic doublet-lattice method, J. of Aircr., Vol. 35, pp. 720-727. https://doi.org/10.2514/2.2382

Roger, K.L., 1977. Airplane math modeling methods for active control design, AGARD Conf. Proc., France, pp. 1-11.

11. RESPONSIBILITY NOTICE

The author(s) is (are) the only responsible for the printed material included in this paper.